Ultrathin Bi(110) films on Si(111)$\sqrt{3} \times \sqrt{3}$-B substrates

Ikuya Kokubo, Yusaku Yoshiike, Kan Nakatsuji, and Hiroyuki Hirayama*

Department of Materials Science and Engineering, Tokyo Institute of Technology, J1-3, 4259 Nagatsuda, Midori-ku, Yokohama 226-8502, Japan

(Received 25 November 2014; revised manuscript received 3 February 2015; published 26 February 2015)

We studied the structure of ultrathin Bi(110) films on Si(111)$\sqrt{3} \times \sqrt{3}$-B substrates using scanning tunneling microscopy. Atomically flat Bi islands were nucleated on the substrates at room temperature. The edges of these islands were parallel to the short side of the Bi(110) rectangular unit cell. The islands extended along six specific orientations because the rectangular Bi(110) and rhombus $\sqrt{3} \times \sqrt{3}$ unit cells were commensurate at the interface. Bi(110) domains along different orientations coexisted and formed various domain boundary structures on the wide terraces of the islands. In particular, the domains along $\pm 87^\circ$ from the $\{1\bar{1}0\}$ direction were connected perfectly on an atomic scale by changing the direction of the *p*-like bond of the in-plane zigzag chains locally at the straight domain boundary. No exclusive preference for the black phosphorus structure was observed for the Bi(110) ultrathin films, in contrast to the islands grown on the Si(111)7 × 7 substrate.

DOI: 10.1103/PhysRevB.91.075429 PACS number(s): 68.37.Ef, 68.55.A−, 68.35.bd

I. INTRODUCTION

Bismuth (Bi) is a group-V semimetal with a rhombohedral (*A*7) crystalline structure in bulk [Fig. 1(a)]. However, theoretical calculations revealed that single bilayer (BL) Bi(111) and Bi(110) films (in rhombohedral indexing hereafter) behaved as insulators [1]. In particular, the Bi(111) BL film was theoretically predicted as a promising candidate for a two-dimensional topological insulator [2,3]. Therefore, much attention has been paid to the growth of ultrathin Bi films.

Substantially, atomically flat, ultrathin Bi islands were obtained from the Bi growth on Si(111)7 × 7 substrates [4–6]. However, the islands with heights of less than 4 monolayers (MLs) had (110)-oriented instead of (111)-oriented surfaces. The Bi(110) islands adopted the pseudomorphic (110)-oriented black phosphorus (BP) structure instead of the *A*7 structure [Fig. 1(b)]. The BP Bi(110) islands were converted to *A*7 Bi(111) islands during further deposition of Bi atoms on the Si(111)7 × 7 substrate.

The Bi(110) islands were also obtained on other substrates in the initial stage of Bi film growth. The Bi(110) islands were distributed randomly and formed a textured in-plane structure on the Si(111)7 × 7 substrates [4,5]. However, Bi(110) islands nucleated along several specific in-plane rotational orientations on W(110) [7], Ge(111)*c*(2 × 8) [8], Si(111)-β-$\sqrt{3} \times \sqrt{3}$-Bi [9,10], highly ordered pyrolitic graphite [11–13], and quasicrystal-surface substrates [14]. It resulted in the formation of quasi-one-dimensional islands in which electrons are confined to reveal quantum size effects [12]. The lattice commensuration at the Bi/substrate interface was suggested as the origin of the preference for specific orientations on W(110) and Si(111)-β-$\sqrt{3} \times \sqrt{3}$-Bi [7,10]. The preference of the BP structure was not remarkable on Ge(111)*c*(2 × 8) and Si(111)-β-$\sqrt{3} \times \sqrt{3}$-Bi substrates [8,9].

In these previous studies, the Bi(110) islands were found to have preferable orientations on several substrates by low-energy electron diffraction, scanning electron microscopy, and electron backscatter diffraction. However, the effect of the substrates on the growth and surface structure of the Bi(110) islands was not analyzed in detail. Furthermore, these Bi(110) domains with different orientations are expected to produce various domain boundary structures on the wide terraces of the Bi(110) islands. However, the details of the arrangement of Bi atoms on the Bi(110) islands with preferred orientations in real space have not been reported. The arrangement of Bi atoms at the domain boundary structure has also not been addressed.

A recent theoretical calculation reveals that the one- and two-BL-thick BP Bi(110) films become nontrivial two-dimensional topological insulators by removing the buckling via substrate-induced strain and charge doping [15]. In addition, a Dirac cone was suggested to be formed at the surface of odd-layer-thick Bi(110) films theoretically [16]. In these respects, the growth, surface structure, and the substrate effect on the Bi(110) ultrathin films are of great importance. In this study, we investigated the details of the atomic arrangements at the Bi(110) islands on the Si(111)$\sqrt{3} \times \sqrt{3}$-B substrate using scanning tunneling microscopy (STM). Though the top atomic layer at this surface is built by Si atoms, the surface is more inert compared to the Si(111)7 × 7 substrate. Thus, one could expect here the growth behavior of Bi films different from that on Si(111)7 × 7 surface which has been studied in a detail. As a result, we found that atomically flat, long, narrow Bi(110) islands extended along specific orientations on this substrate. The orientations belonged to one of the two sets of threefold rotational axes. The orientations in one set differed by 26° to the orientations in the other set because of the commensurate alignment of the diagonal of the rectangular Bi(110) lattice to that of the $\sqrt{3} \times \sqrt{3}$ unit cell at the substrate. The Bi(110) islands extended along the short side of the rectangular cells. Depending on the combination of the Bi domains with different orientations, several types of boundaries appeared on the wide terraces of the Bi(110) islands. In particular, the domains along $\pm 87^\circ$ from the $\{1\bar{1}0\}$ direction were connected perfectly on the atomic scale at the straight boundary by inserting a local switching of the bond direction to the zigzag chains of the in-plane bonds. No exclusive preference for the BP structure was observed for the Bi(110) islands on the Si(111)$\sqrt{3} \times \sqrt{3}$-B substrate.

*hirayama.h.aa@m.titech.ac.jp

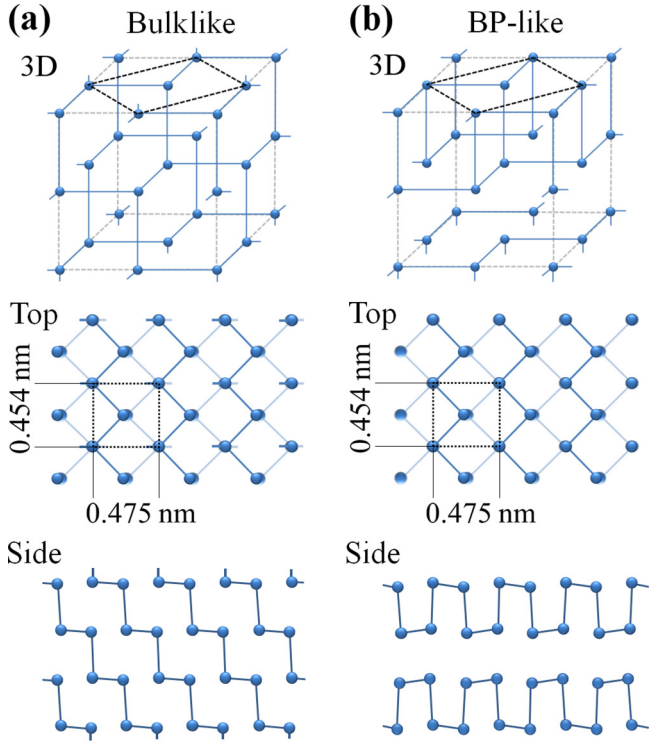

FIG. 1. (Color online) Structural models of the Bi(110) island with $A7$ (a) and BP (b) structures. Top: Three-dimensional (3D) image. Middle: top view. Bottom: side view. The Bi atoms are indicated by filled circles. The bonds between Bi atoms are indicated by solid lines. Each Bi atom has three p-like bonds: one out-of-plane and two in-plane bonds. Note that the in-plane bonding in the top and the second layer are distinguished by thick and thin lines in the top view. The rectangular unit cell is also indicated by black dashed lines in the top view.

II. EXPERIMENT

Experiments were conducted in an ultrahigh vacuum (UHV) apparatus with a Bi Knudsen cell and an STM [17]. Si(111)$\sqrt{3} \times \sqrt{3}$ substrates were prepared by flashing highly B-doped Si(111) samples at 1523 K for 5 s and subsequently annealing them at 1223 K for 10 min [18]. The Bi atoms were deposited on the substrates at a rate of 0.056 ML/min at room temperature. The growth rate was calibrated by the deposition time to complete the Bi-induced $\sqrt{3} \times \sqrt{3}$ reconstruction with 1/3 ML Bi atoms at the Ag(111) surfaces [19]. The structure of the Bi films was characterized with STM. STM tips were electrochemically etched from polycrystalline tungsten wires. The tips were cleaned by electron bombardment in the UHV apparatus. During STM, the sample was cooled to 70 K by a supercooled liquid-nitrogen cryostat attached to the STM unit, and a bias voltage (V) was applied to the sample. The $\{1\bar{1}0\}$ and $\{11\bar{2}\}$ directions of the Si(111)1×1 lattice were determined using the alignment of the protrusions in the STM image of the Si(111)$\sqrt{3} \times \sqrt{3}$-B substrates. The in-plane orientation of the Bi(110) islands and domains were determined by the angle to the $\{1\bar{1}0\}$ and $\{11\bar{2}\}$ axes in the STM images. These orientations were also checked in the fast Fourier transform (FFT) pattern of the STM images. STM images were taken after thermal drift fully subsided.

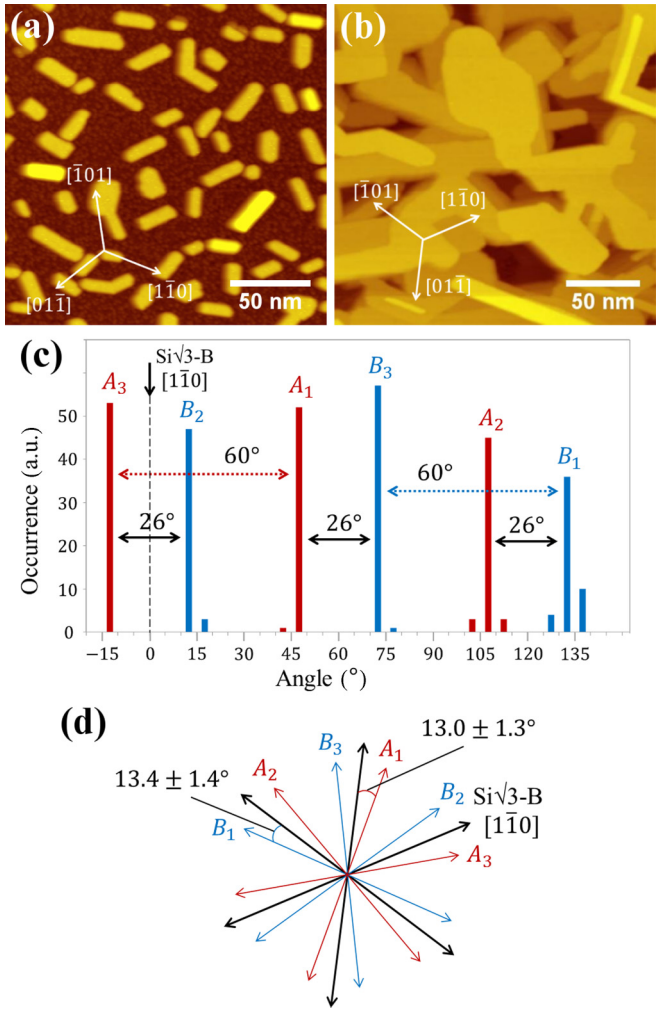

FIG. 2. (Color online) STM image of Bi films after (a) 1 ML and (b) 2 ML Bi deposition at room temperature on the Si(111)$\sqrt{3} \times \sqrt{3}$-B substrates. The size of the image is (a) 200 × 200 nm and (b) 217 × 217 nm. The images were taken with a bias voltage (V) of +2.0 V and a tunneling current (I) of 0.1 nA at the temperature of liquid nitrogen. (c) Distribution of the in-plane orientation of the needlelike islands obtained for the 1 ML Bi deposition. The rotational angle was measured from the $[1\bar{1}0]$ direction of the Si(111)1×1 substrate lattice. The preferred orientations are referred to as A_is and B_is in the following description. (d) Polar diagram of the preferred orientations of the Bi islands.

III. RESULTS AND DISCUSSION

A. Preferential orientations of the Bi(110) islands

Atomically flat, long, narrow islands were nucleated by depositing Bi atoms on the Si(111)$\sqrt{3} \times \sqrt{3}$-B substrate. Figure 2(a) shows an STM image after 1 ML Bi deposition. The islands extend along specific orientations close to the threefold rotational $\{1\bar{1}0\}$ directions. However, detailed analysis revealed that the islands have six preferential orientations, as shown in the histogram of the frequency of the orientations in Fig. 2(c). The preferred orientations belong to two sets of threefold rotational axes (red and blue bars) which differed by 26°. The islands widened during further Bi deposition [Fig. 2(b)]. However, they still maintained the six preferred orientations.

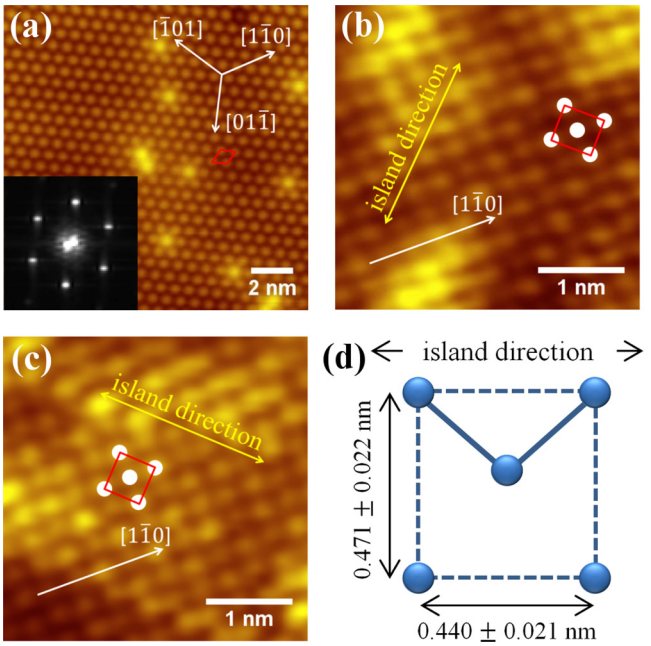

FIG. 3. (Color online) STM images of (a) Si(111)$\sqrt{3} \times \sqrt{3}$-B substrate, and the Bi(110) islands with a height of 6 MLs extending in the (b) A_1 and (c) B_1 orientations. The direction of the islands and the $\{1\bar{1}0\}$ orientation are indicated by yellow and white arrows in the STM images, respectively. The image size is 14.5 × 14.5 nm in (a), and 3.5 × 3.5 nm in (b) and (c). $V = +2.0$ V in (a), -0.2 V in (b), and -0.3 V in (c). $I = 0.1$ nA in (a) and 0.3 nA in (b) and (c). (d) Unit cell of the Bi atom arrangement. Bi atoms are arranged with a centered rectangular unit cell regardless of the orientation. The experimentally obtained sizes of the long and short sides of the unit cell are shown in the schematic. The direction of the Bi(110) islands along the short side of the unit cell is indicated by the black arrow.

Atomically resolved STM images of the pristine Si(111)$\sqrt{3} \times \sqrt{3}$-B substrate and the grown Bi islands are shown in Fig. 3. Protrusions appear at the top surface Si atoms on the S_5 subsurface B sites on the Si(111)$\sqrt{3} \times \sqrt{3}$-B substrate [Fig. 3(a)] [20,21]. The small number of bright protrusions reflects the defect sites at which the S_5 subsurface sites are not displaced by B atoms [21]. The number of defect sites is less than 2% on the Si(111)$\sqrt{3} \times \sqrt{3}$-B substrate. Figures 3(b) and 3(c) show the arrangement of Bi atoms on the islands extending in A_1 and B_1 orientations. Islands of various heights were nucleated by depositing a few MLs of Bi atoms (see Sec. III C). However, the atomic arrangement on the islands does not depend on the island height. The figures show the STM images of the islands with a height of 6 MLs. The Bi atoms are arranged periodically by repeating the centered rectangular unit cells (indicated by white dots) regardless of the orientation. The STM images show that the long and short sides of the rectangular unit cell are 0.471 ± 0.022 and 0.440 ± 0.021 nm [Fig. 3(d)], respectively. The truncated Bi(110) surface has the same atomic arrangement with a centered rectangular unit cell in the $A7$ and BP structures [Figs. 1(a) and 1(b)]. The shape and size of the centered unit cell in the STM images [Fig. 3(d)] are identical to those of the bulk-truncated $A7$ and BP Bi(110) surfaces (0.475 × 0.454 nm; Fig. 1) [4]. Thus, these islands on the

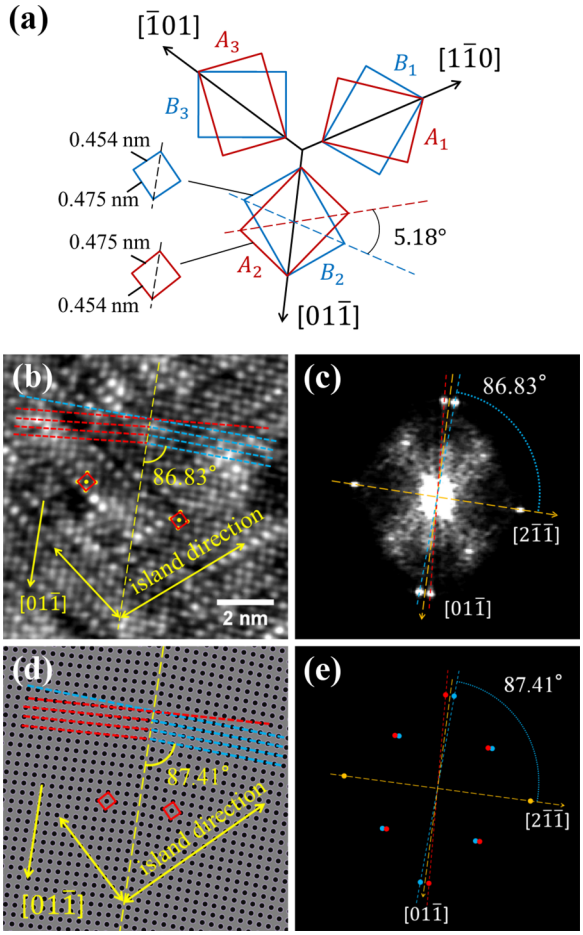

FIG. 4. (Color online) (a) Possible ways to place the diagonal of the Bi(110) rectangular unit cell on the $\{01\bar{1}\}$ axes. For each $\{01\bar{1}\}$ axis, there are two ways to place the diagonal of the rectangular unit cell (A in red and B in blue). The rectangular unit cells are distorted to illustrate the placement more clearly. The rectangular unit cells with the actual length ratio are shown on the lower left. (b) STM image of a terrace on the 5-ML-high Bi(110) islands. The unit cell is indicated by the red rectangle with yellow dots. A_2 and B_2 Bi(110) domains are bounded at the straight boundary along the $[01\bar{1}]$ direction (yellow dashed line). The directions in which the two domains extend are indicated by yellow arrows. The image sizes are 10 × 10 nm. $V = -0.1$ V, $I = 0.3$ nA. (c) FFT pattern of the STM image in (b). (d) Sketch of the protrusions in the STM image in (b). The unit cell is indicated by the red rectangle. (e) Reciprocal points that were calculated for the two domains in (d).

Si(111)$\sqrt{3} \times \sqrt{3}$-B substrates were assigned as the Bi(110) islands. The islands extend along the short side of the unit cell (indicated by yellow arrows) in A_1 and B_1 orientations [Figs. 3(b) and 3(c)]. The same relation between the unit cell and side also holds in the islands extending other orientations (A_2, A_3 and B_2, B_3).

The rectangular shape of the unit cell explains why there are two preferred sets of threefold orientations that differ by 26°. Figure 4(b) shows an STM image of the terrace of a 5-ML-high Bi(110) island. The atoms appear to align with the same periodicity over the whole STM image. However, on further inspection, there are two Bi(110) domains in the STM image. The two domains are bounded along the $\{01\bar{1}\}$ direction

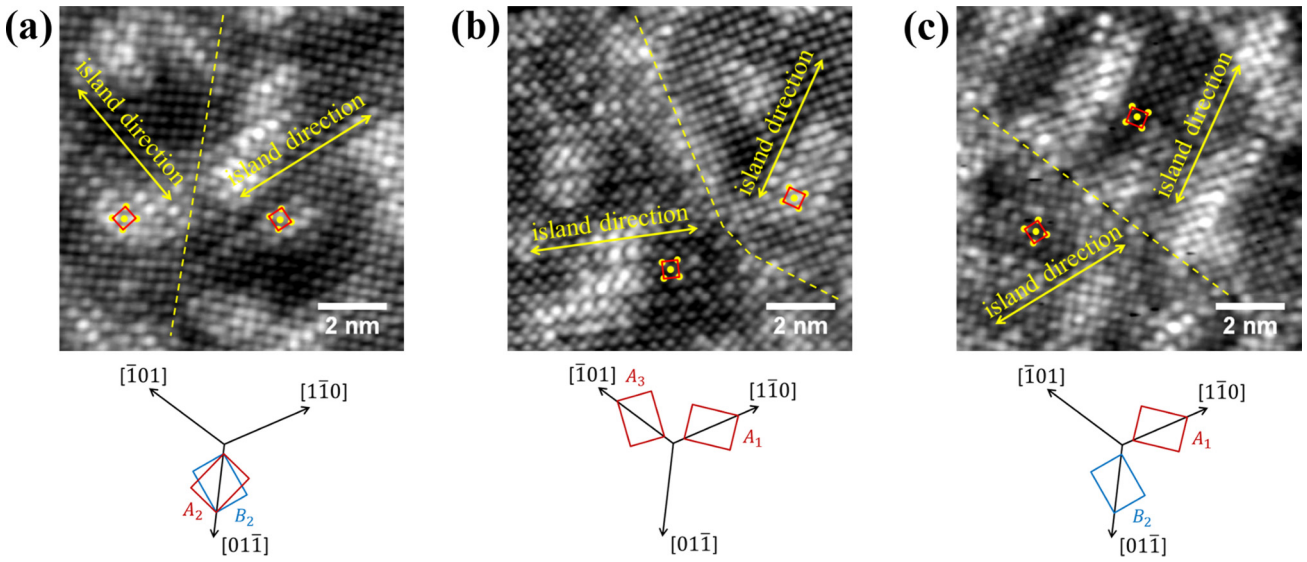

FIG. 5. (Color online) STM images of the boundaries between different types of domain (10×10 nm, $V = -0.1$ V, $I = 0.3$ nA). Boundary between (a) A_2-B_2 domains, (b) A_1-A_3 domains, and (c) A_1-B_2 domains. The boundaries are indicated by yellow dashed lines. The unit cell is indicated by the red rectangle with yellow dots (Bi atoms) in each domain. The directions in which the islands extend are indicated by yellow arrows.

(dashed line). Their lattices (red and blue lines) are tilted by 6° (angle made by the red and blue lines). This tilt angle arises from the two ways in which the diagonal of the Bi(110) rectangular unit cell can be placed on the {01$\bar{1}$} line. The diagonal in the vertical direction is parallel to the {01$\bar{1}$} boundary in both the left and right domains, as shown in the STM image and its schematics [Figs. 4(b) and 4(d)]. However, the diagonal of the rectangular unit cell can be placed on the {1$\bar{1}$0} orientation in two ways [red and blue rectangles in Fig. 4(a)]. This results in the rotation of the other diagonal by 5.18° for the rectangular unit cell with the size shown in Fig. 1. This rotation angle is consistent with that observed in STM. In the meantime, the sides of the unit cells with the diagonals in the [01$\bar{1}$] and [1$\bar{1}$0] directions make an angle of $120 - (45 \times 2) = 30°$ by assuming the unit cell is square. However, the short side is shifted by a further 1.295° from 45° for the rectangular unit cell. As a result, the angle between the short sides of the rectangular unit cells is reduced to $30 - (1.295 \times 2) = 27.41°$. The islands are extended parallel to the short side of the unit cell. Therefore, the two ways to place the diagonal of the rectangular unit cell explain reasonably the appearance of the two sets of the preferential orientations of the Bi(110) islands that differ by 26°. The FFT of the STM image in Fig. 4(c) confirms the two diagonal placements; the spots are split along the {01$\bar{1}$} line. Figure 4(e) shows the calculated reciprocal lattices for the two rectangular unit cells with diagonals placed on the {01$\bar{1}$} line in the two different ways. The spots in the FFT are reproduced well in the calculation assuming there are two ways to place the diagonal of the rectangular unit cell.

The diagonal of the Bi(110) unit cell is preferentially placed on the {1$\bar{1}$0} orientation because of the lattice commensuration. The {1$\bar{1}$0} direction is parallel to the diagonal of the rhombus unit cell of the Si(111)$\sqrt{3} \times \sqrt{3}$-B lattice at the substrate. The diagonal of the $\sqrt{3} \times \sqrt{3}$-B unit cell (1.152 nm) is commensurate to that of the Bi(110) unit cell diagonal (0.657 nm) with a whole number ratio of 4:7 (4.607 vs 4.599 nm). We consider that this commensuration drives the placement of the Bi(110) lattice diagonal in the {1$\bar{1}$0} direction.

B. Boundaries between Bi(110) domains with different orientations

The Bi(110) domains along different orientations coexist on the wide terraces of the Bi(110) islands. The variety of domain boundary structures arises from combinations of the orientations of adjacent domains. The orientations of the domains are determined by (i) the choice of the {1$\bar{1}$0} axis (i.e., [01$\bar{1}$], [$\bar{1}$01], or [1$\bar{1}$0]) and (ii) the placement of the unit-cell diagonal on the axes [A_i (red) or B_i (blue)] as shown in Fig. 4(a). Figures 5(a)–5(c) show three typical combinations of adjacent domain orientations: A and B cells on the same {1$\bar{1}$0} (ith) axis; the same type of cells (A-A or B-B) on different (i- and j-) {1$\bar{1}$0} axes; and different types of cells (A-B) on different (i- and j-) {1$\bar{1}$0} axes. All these combinations are visible on the terraces of the Bi(110) islands in the STM images, as shown in the upper column in Fig. 5.

In the STM images, the domain boundaries extend in the {1$\bar{1}$0} or {11$\bar{2}$} directions in these domain structures. In particular, the boundaries along {1$\bar{1}$0} are straight [Figs. 5(a) and 5(c)]. In Fig. 5(b), the {1$\bar{1}$0} boundary (in the lower right) is connected to the {11$\bar{2}$} boundary (upper half) in a smooth, obtuse manner. The ordering of the atomic arrangements is maintained in the domains of both sides up to the boundaries in all cases.

Figures 6(a)–6(c) show the magnified STM images of the corresponding boundaries in Figs. 5(a)–5(c). The arrangement of atoms is perfectly continuous at the boundary in Fig. 6(a). We propose the following explanation for this observation. A Bi atom has three p-like bonds. In the Bi(110) islands, two bonds extend in the (110) plane (generally along the x and y axis), whereas the other bond lies in the out-of-plane (z-axis) direction, in both the $A7$ and BP Bi(110) structures (Fig. 1).

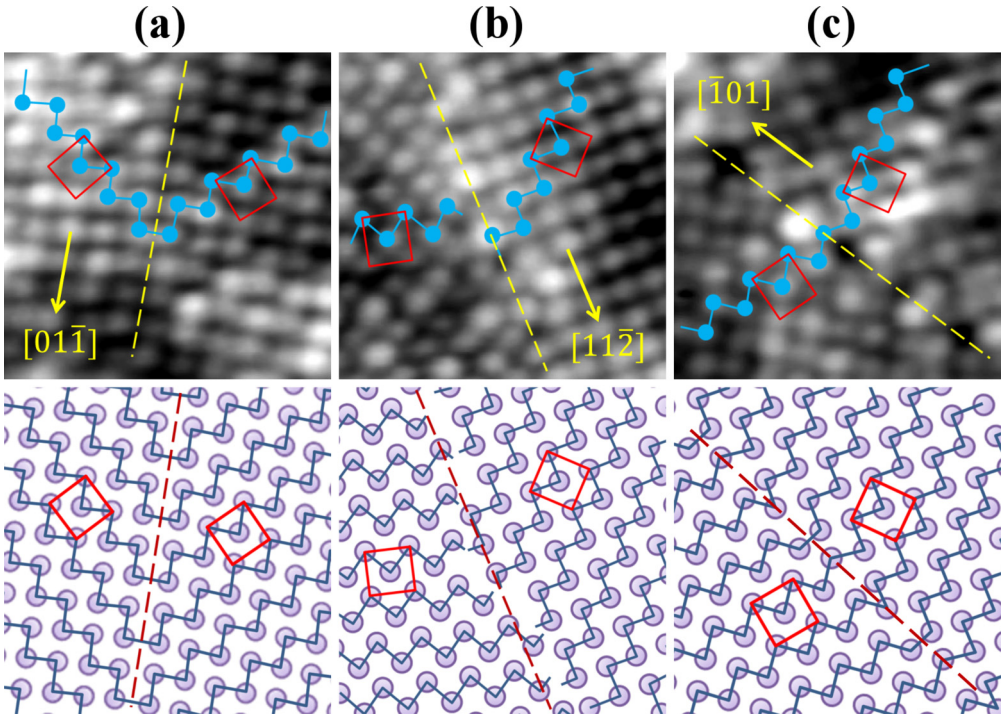

FIG. 6. (Color online) Magnified STM images of the domain boundaries in Fig. 5 (3.5 × 3.5 nm, $V = -0.1$ V, $I = 0.3$ nA). (a) A_2-B_2 domain boundary. (b) A_1-A_3 domain boundary. (c) A_1-B_2 domain boundary. The schematics below are sketches of the protrusions in the STM images. The domain boundaries are indicated by yellow and red dashed lines. The unit cells are indicated by red rectangles. In the STM images, the in-plane zigzag bonds are indicated by solid lines. The Bi atoms in the zigzag chain are overlaid with blue dots and lines. The bonds connect the adjacent atoms to maintain the zigzag chains where possible for the atoms at the boundaries.

The Bi atoms form a zigzag chain, which is the basic element of the in-plane atomic arrangement, by alternating the bonds along the x and y directions. The zigzag chain is formed by the alternation of $+x$ and $-y$ oriented bonds in the left domain [Fig. 6(a)], whereas the chain is formed by the alternation of $+x$ and $+y$ oriented bonds in the right domain. The alternation of the bonds is switched from $-y$ to $+y$ on only the Bi atoms at the $\{1\bar{1}0\}$ straight boundary. However, the Bi atom at the boundary still maintains the p-bond scheme locally, in which the in-plane bonds extend along the x and y directions. Thus, the zigzag chain on the left side can be connected to that on the right side with perfect continuity at the boundary, as in Fig. 5(a). The key to the continuity is the flexibility of the orientation of the bond along the y direction.

The zigzag chains in the right and left domains are symmetric about the $\{1\bar{1}0\}$ straight boundary in Fig. 6(a). This is also true of the domains in Fig. 4(c). However, the angle of the zigzag chains to the boundary in Fig. 6(c) is different from that in Fig. 6(a). In Fig. 6(a), the left chain makes an angle of -45° with the boundary. Thus, when switching from the $-y$ to the $+y$ bond, a zigzag chain in the right domain can connect with an angle of $+45^\circ$. However, the angle deviates from 45° in Fig. 6(c). Thus, the boundary atoms must distort their in-plane bonds to connect the zigzag chains from both sides. In the sketch of the protrusions in the lower column of Fig. 6(c), the distorted zigzag bonds are overlaid on the boundary atoms as solid lines to make the zigzag chains on both sides continuous. These distorted bonds should cost energy, and it is not clear whether the Bi atoms could adopt the distorted p-bond scheme at the boundary. However, some of the boundary atoms show bonding similar to that at the boundary in Fig. 6(a). This reduces the tension of the $\{1\bar{1}0\}$ boundary and helps it to extend straight [Fig. 6(c)].

At the boundary in Fig. 6(b), the zigzag chains are not symmetric about the $\{1\bar{1}0\}$ boundary. The zigzag chains on both sides cannot be connected continuously by modifying the in-plane bond angles of the Bi atoms at the boundary [Fig. 6(b), lower column]. As a result, some zigzag chains are left truncated at the boundary. Thus, this $\{1\bar{1}0\}$ boundary does not extend further, and bends easily [Fig. 5(b)].

C. Nonremarkable preferences of the BP structure

The Bi(110) islands with $A7$ and BP structures show the same atomic arrangement with the centered rectangular unit cell shown in Fig. 3(d). However, the Bi(110) islands with the BP structure are composed of stacked double layers [Fig. 1(b), lower column]. Thus, the BP Bi(110) islands have only even ML heights. In contrast, the $A7$ Bi(110) islands, in which every layer is connected vertically [Fig. 1(a), lower column] have both odd and even ML heights. Figure 7(a) shows the distribution of the heights of the Bi(110) islands on the Si(111)$\sqrt{3} \times \sqrt{3}$-B substrates after 2 ML Bi deposition. The islands mainly have ML heights of 4, 5, and 6. There is no preference for the even ML heights at any Bi coverage. This means that the BP Bi(110) islands are not strongly preferred on Si(111)$\sqrt{3} \times \sqrt{3}$-B substrates.

However, the relative height of the center atom to the corner atoms in the Bi(110) rectangular unit cell is different for the even and odd ML island heights. The center atom is lower

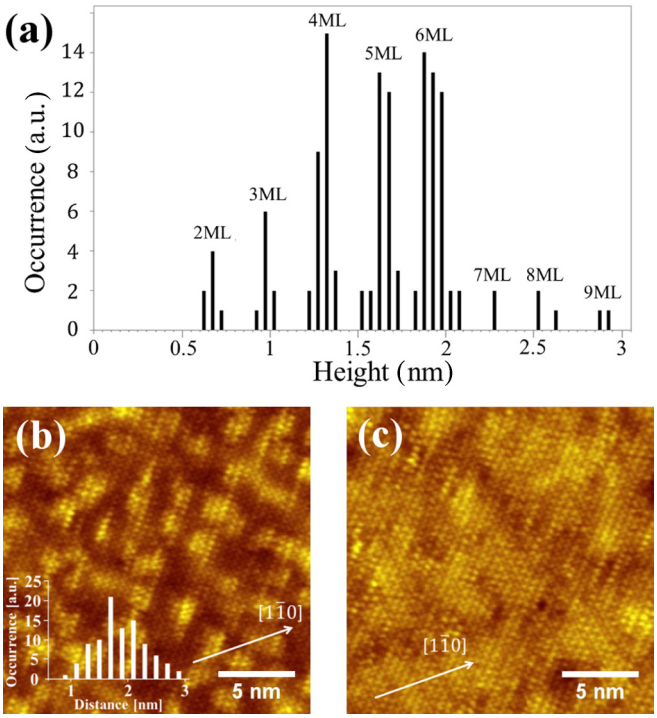

FIG. 7. (Color online) (a) Height distribution of the Bi(110) islands obtained from the 2-ML Bi deposition on the Si(111)$\sqrt{3} \times \sqrt{3}$-B substrate. (b),(c) Wide-range STM images of the Bi(110) islands with heights of (b) 6 and (c) 5 MLs, 20 × 20 nm, $V = -0.6$ V, $I = 0.3$ nA. The long-range modulation of the contrast is overlaid on the periodic arrangement of Bi atoms on the 6-ML Bi(110) islands (b). The distances between the bright regions in the contrast modulation are displayed in the histogram in the inset in (b).

than the corner atoms by 0.031 nm on the 6-ML-high Bi(110) islands, whereas it is only 0.016 nm lower on the 5-ML-high Bi islands. Corrugation is remarkably observed at any bias voltage on only the even ML height islands. The corrugation at the 6-ML-high islands is consistent with that reported for the BP Bi(110) island surface in a previous study (0.032 nm) [22]. In addition, it was reported that the corrugation on the $A7$ Bi(110) surface is much smaller than that on the BP Bi(110) surface [4,23]. Thus, the 6-ML-high Bi(110) islands have a BP structure, whereas the 5-ML-high Bi(110) islands have an $A7$ structure. However, it remains an open question whether the Bi(110) islands change their structure from $A7$ to BP and vice versa as the number of MLs increases during the growth on the Si(111)$\sqrt{3} \times \sqrt{3}$-B substrates.

In addition to the corrugation in the unit cell, the STM image in Fig. 7(b) shows that a remarkable long-range scale modulation overlaps the Bi lattice on the even ML height Bi(110) islands. The modulation, which does not have a particular periodicity, is observed on the even ML height islands regardless of the bias voltage. However, a bright contrast area appears with an average interval of about 2 nm. The vertical amplitude of the modulation is about 0.06 nm. No unusual modulation is visible on the odd ML height Bi(110) islands in Fig. 7(c). The origin of the modulation of the even ML height Bi(110) islands is not known at present.

The Bi(110) islands extend along the short side of the rectangular unit cell regardless of the height and structure. The short side is parallel and the long side is perpendicular to the zigzag chain on the Bi(110) surfaces with the $A7$ and BP structures (Fig. 8, upper column). In the side views (Fig. 8, lower column), the number of dangling bonds protruding to the vacuum side appears to be smaller on the short side edge

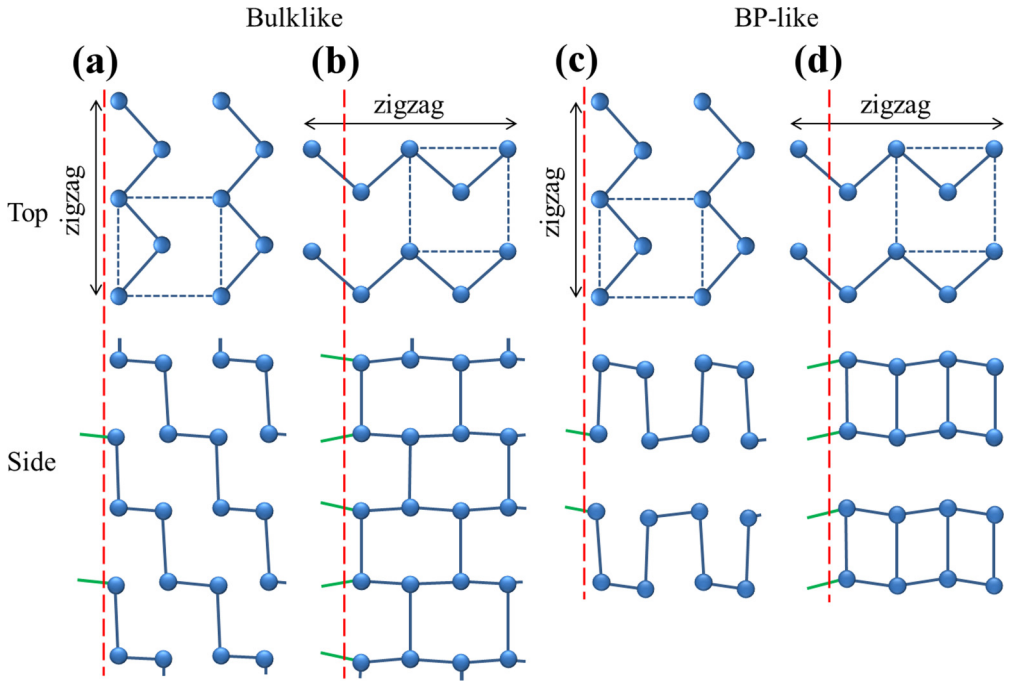

FIG. 8. (Color online) Structural model of the atomic arrangement at the edge of the Bi(110) islands with $A7$ (a),(b) and BP (c),(d) structures. Upper panel: top view. Lower panel: side view. The edge, indicated by the red line, is along the short side of the unit cell in (a) and (c), and along the long side of the unit cell in (b) and (d). The Bi atoms and their bonds are indicated by circles and short lines. The zigzag chains are parallel to the short side.

[(a) and (c)] than the long side edge [(b) and (d)] in both the *A*7 and BP Bi(110) islands. However, each atom at the very edge has two dangling bonds on the short side, in contrast to one dangling bond on the long side. Thus, the short and long sides show no difference in the number of energetically unfavorable dangling bonds. Consequently, the Bi(110) islands extend along the short side not because of an energetic reason but because of the growth kinetics. Substantially, the Bi atoms are involved in the bonds in the zigzag chain, whereas the atoms in adjacent chains are not bonded directly in plane. Therefore, the migrating atoms should be attached to the end of the zigzag chain during growth. As a result, the islands extend along the zigzag chain. This explains why the islands have longer edges along the short side of the unit cell in both *A*7 and BP Bi(110).

IV. SUMMARY

In summary, we studied the atomic arrangements on the terraces of Bi(110) islands on Si(111)$\sqrt{3} \times \sqrt{3}$-B substrates. The nucleation of atomically flat Bi(110) islands was observed. The islands extended preferentially along specific orientations, which belonged to one of two threefold rotational axes that differed by 26°. The islands extended so as the short side of the rectangular unit cell was aligned in the preferential direction. The preferred directions were explained by the fact that the diagonal of the $\sqrt{3} \times \sqrt{3}$-B unit cell (1.152 nm) is commensurate to that of the Bi(110) unit cell (0.657 nm) with a ratio of 4:7. This commensuration and the two possible ways to place the diagonal of the rectangular Bi(110) unit cell resulted in the two sets of threefold rotational axes for the direction in which the Bi(110) islands extended. Bi(110) domains with different orientations met and formed boundaries on wide terraces. In particular, two domains rotated by 87° along the same $\{01\bar{1}\}$ orientation formed a perfectly continuous straight boundary by switching the in-plane bond orientation in the zigzag chain locally at the boundary. On the Si(111)$\sqrt{3} \times \sqrt{3}$-B substrates, both the BP Bi islands with an even ML height and large surface corrugation and the bulklike Bi(110) islands with an odd ML height and small surface corrugation appeared. No exclusive preference was observed for the even ML height islands on the Si(111)$\sqrt{3} \times \sqrt{3}$-B substrates.

[1] Y. M. Koroteev, G. Bihlmayer, E. V. Chulkov, and S. Blügel, Phys. Rev. B **77**, 045428 (2008).

[2] S. Murakami, Phys. Rev. Lett. **97**, 236805 (2006).

[3] M. Wada, S. Murakami, F. Freimuth, and G. Bihlmayer, Phys. Rev. B **83**, 121310(R) (2011).

[4] T. Nagao, J. T. Sadowski, M. Saito, S. Yaginuma, Y. Fujikawa, T. Kogure, T. Ohno, Y. Hasegawa, S. Hasegawa, and T. Sakurai, Phys. Rev. Lett. **93**, 105501 (2004).

[5] J. T. Sadowski, T. Nagao, S. Yaginuma, Y. Fujikawa, T. Sakurai, A. Oreshkin, M. Saito, and T. Ohno, J. Appl. Phys. **99**, 014904 (2006).

[6] S. Yaginuma, K. Nagaoka, T. Nagao, G. Bihlmayer, Yu. M. Koroteev, E. V. Chulkov, and T. Nakayama, J. Phys. Soc. Jpn. **77**, 014701 (2008).

[7] C. Koitzsch, M. Bovet, F. Clerc, D. Naumovic, I. Schlapbach, and P. Aebi, Surf. Sci. **527**, 51 (2003).

[8] S. Hatta, Y. Ohtsubo, A. Miyamoto, H. Okuyama, and T. Aruga, Appl. Surf. Sci. **256**, 1252 (2009).

[9] S. Yaginuma, T. Nagao, J. T. Sadowski, M. Saito, K. Nagaoka, Y. Fujikawa, T. Sakurai, and T. Nakayama, Surf. Sci. **601**, 3593 (2007).

[10] D. Lükermann, S. Banyoudeh, C. Brand, S. Sologub, H. Pfnür, and C. Tegenkamp, Surf. Sci. **621**, 82 (2014).

[11] S. A. Scott, M. V. Kral, and S. A. Brown, Surf. Sci. **587**, 175 (2005).

[12] P. J. Kowalczyk, O. Mahapatra, D. N. McCarthy, W. Kozlowski, Z. Klusek, and S. A. Brown, Surf. Sci. **605**, 659 (2011).

[13] P. J. Kowalczyk, D. Belic, O. Mahapatra, S. A. Brown, E. S. Kadantsev, T. K. Woo, B. Lngham, and W. Kozlowski, Appl. Phys. Lett. **100**, 151904 (2012).

[14] H. R. Sharma, V. Fournée, M. Shimoda, A. R. Ross, T. A. Lograsso, P. Gille, and A. P. Tsai, Phys. Rev. B **78**, 155416 (2008).

[15] Y. Lu, W. Xu, M. Zeng, G. Yao, L. Shen, M. Yang, Z. Luo, F. Pan, K. Wu, T. Das, P. He, J. Jiang, J. Martin, Y. P. Feng, H. Lin, and X. Wang, Nano Lett. **15**, 80 (2015).

[16] G. Bian, X. Wang, T. Miller, T.-C. Chiang, P. J. Kowalczyk, O. Mahapatra, and S. A. Brown, Phys. Rev. B **90**, 195409 (2014).

[17] H. Fukumoto, Y. Aoki, and H. Hirayama, Phys. Rev. B **86**, 165311 (2012).

[18] Y. Yoshiike, H. Fukumoto, I. Kokubo, Y. Aoki, K. Nakatsuji, and H. Hirayama, Appl. Phys. Lett. **104**, 191605 (2014).

[19] J. Hejtmánek, E. Šantavá, K. Knížek, M. Maryško, Z. Jirák, T. Naito, H. Sasaki, and H. Fujishiro, Phys. Rev. B **82**, 165107 (2010).

[20] E. Kaxiras, K. C. Pandey, F. J. Himpsel, and R. M. Tromp, Phys. Rev. B **41**, 1262 (1990).

[21] I.-W. Lyo, E. Kaxiras, and Ph. Avouris, Phys. Rev. Lett. **63**, 1261 (1989).

[22] J.-T. Sun, H. Huang, S. L. Wong, H.-J. Gao, Y. P. Feng, and A. T. S. Wee, Phys. Rev. Lett. **109**, 246804 (2012).

[23] J. Sun, A. Mikkelsen, M. Fuglsang Jensen, Y. M. Koroteev, G. Bihlmayer, E. V. Chulkov, D. L. Adams, P. Hofmann, and K. Pohl, Phys. Rev. B **74**, 245406 (2006).